Electronic Supplementary Material (ESI) for Physical Chemistry Chemical Physics.

Supporting Information

Theoretical study on superconductivity of graphene-like TMB_6 (TM = Cr, Fe and Co) monolayer and its potential anchoring and catalytic properties for Lithium-Sulfur batteries

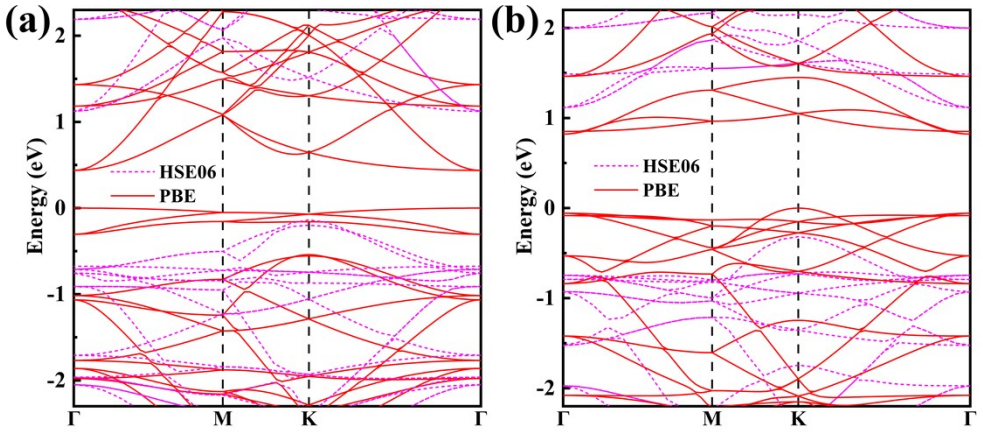

Figure S1. The electronic band structure of (a) FeB_6 and (b) CrB_6 were calculated by using PBE and HSE06. The Fermi energy have been shifted to zero.

Table S1 Calculated parameters of C_{ij} ($N \cdot m^{-1}$), Young's modulus ($N \cdot m^{-1}$) and the Poisson's ratio for CoB_6, FeB_6 and CrB_6.

Compounds	C_{11}	C_{12}	C_{13}	C_{33}	C_{44}	C_{66}	$Y_{x/y}$	$\nu_{x/y}$
CoB_6	159.6	55.5	0.14	0.13	0.01	52.05	140.3	0.35
FeB_6	177.4	48.6	0.71	1.53	3.72	64.4	164.1	0.27
CrB_6	106.9	9.4	0.26	0.01	0.01	48.75	106.1	0.09

Table S2 Corresponding total energy (eV) of per unit cell and magnetic moment (μ_B) in CoB_6, FeB_6 and CrB_6.

Compounds	Configuration	Energy (eV)	Magnetic moment (μ_B)
CoB_6	Nonmagnetic	-42.5407	0
	FM	-42.5407	0
	AFM-Zigzag	-42.5407	0
	AFM-Stripy	-42.5407	0
FeB_6	Nonmagnetic	-43.9771	0
	FM	-43.9771	0
	AFM-Zigzag	-43.9771	0
	AFM-Stripy	-43.9771	0
CrB_6	Nonmagnetic	-44.4806	0
	FM	-44.4806	0
	AFM-Zigzag	-44.4806	0
	AFM-Stripy	-44.4806	0

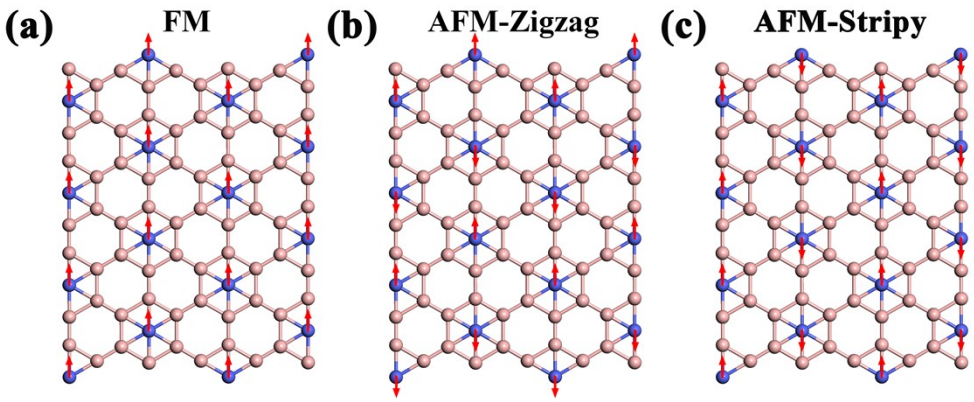

Figure S2 Possible magnetic configurations of TMB_6 monolayers. The spin-up and spin-down orientations are indicated by the up and down arrows, respectively.

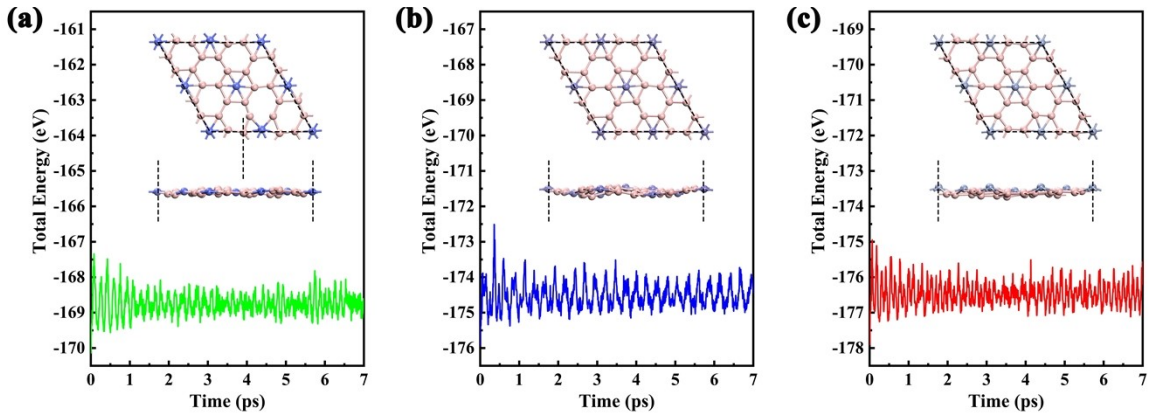

Figure S3. The variations of the total energy of (a) CoB_6, (b) FeB_6, and (c) CrB_6 at 400 K during the AIMD simulations. The insets are the top and side views of the last structural snapshots.

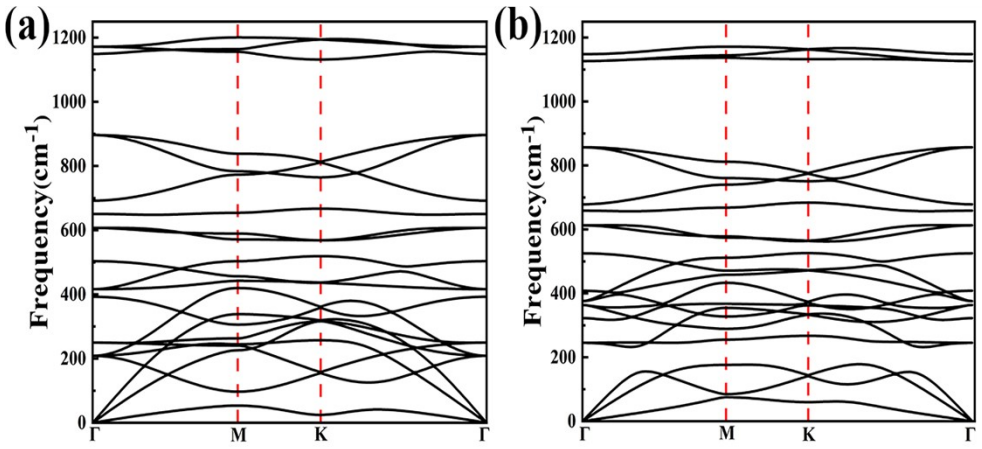

Figure S4. Phonon dispersions of (a) FeB_6 and (b) CrB_6.

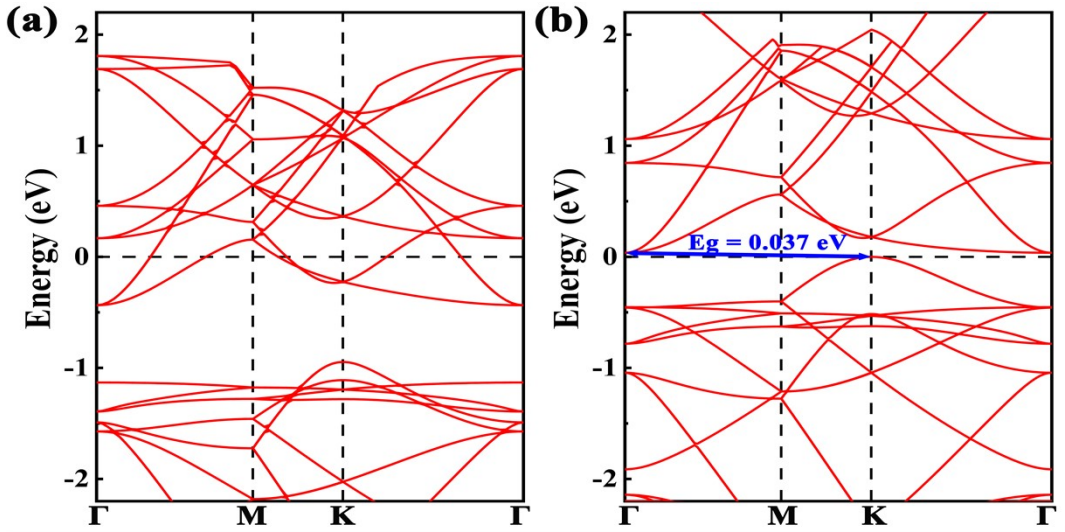

Figure S5. The electronic band structure of (a) original CoB_6 and (b) CoB_6 removed four electrons.

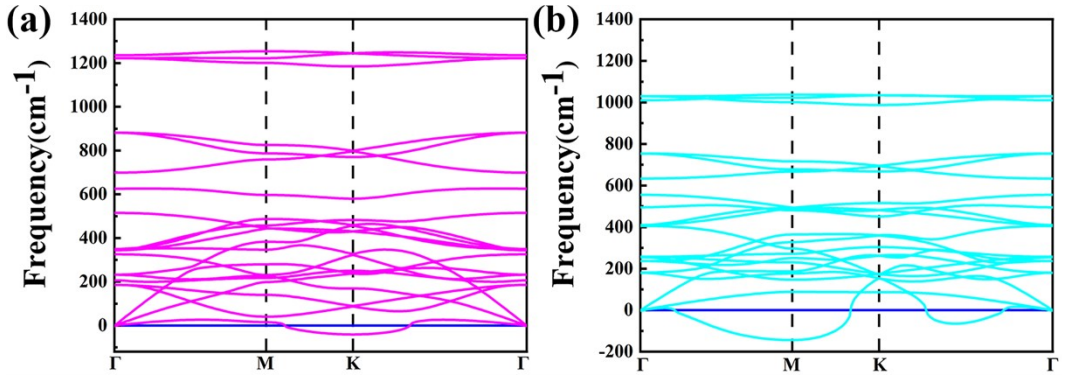

Figure S6. Effect of biaxial strain on phonon dispersions for CoB_6 under (a) strain= -1% and (b) strain = 3%.

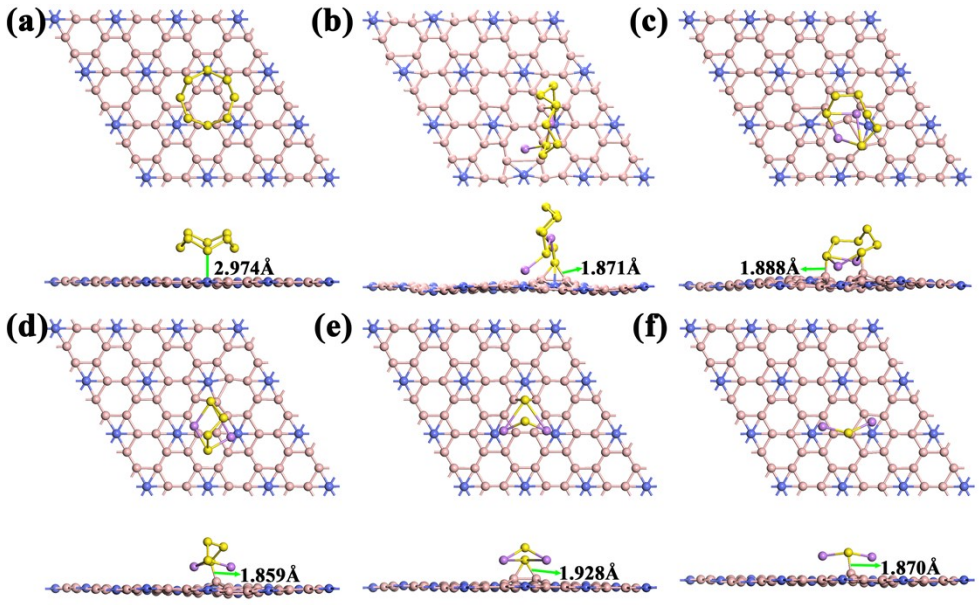

Figure S7. Top and side view of the optimized structures of S_8 and Li_2S_n on CoB_6 monolayer.

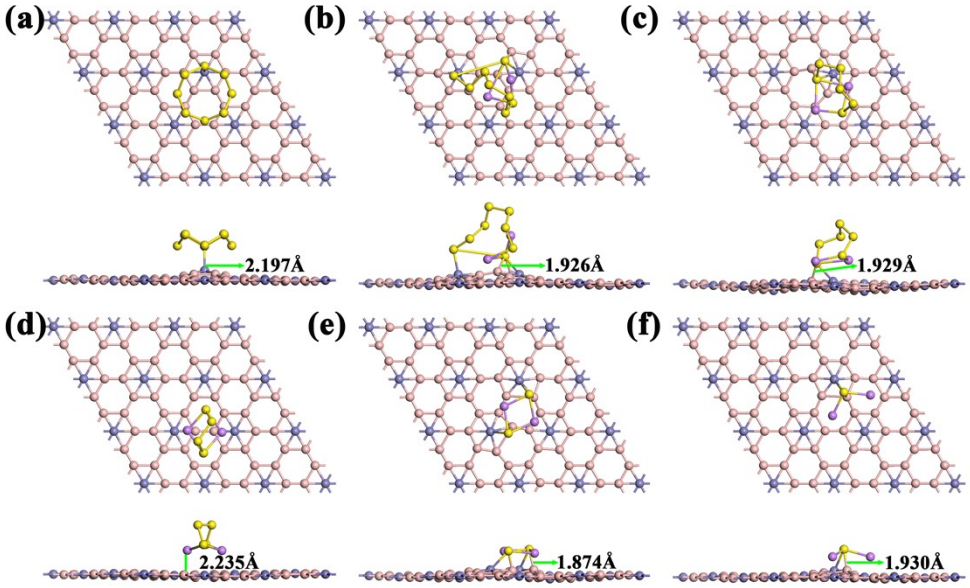

Figure S8. Top and side view of the optimized structures of S_8 and Li_2S_n on FeB_6 monolayer.

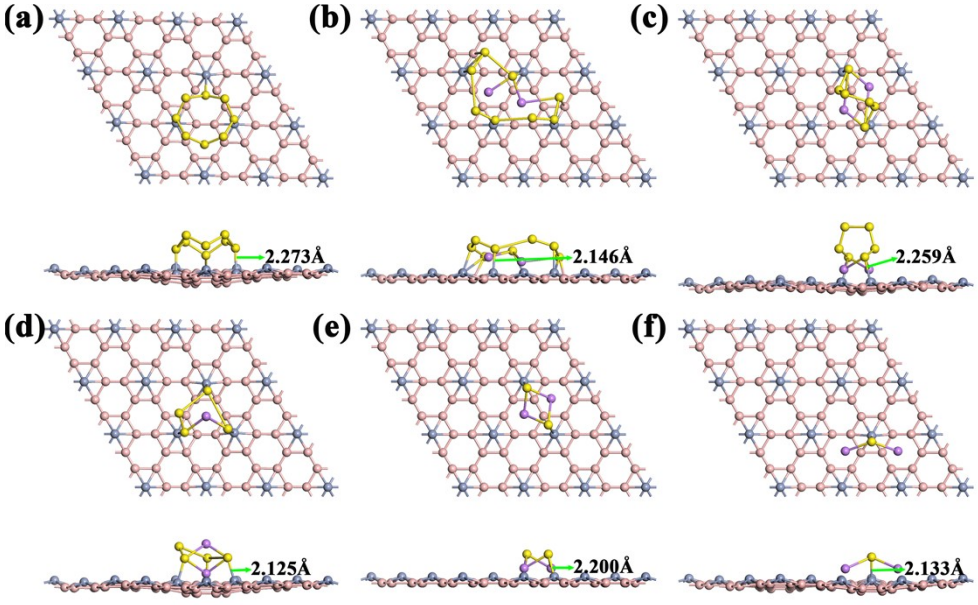

Figure S9. Top and side view of the optimized structures of S_8 and Li_2S_n on CrB_6 monolayer.

Table S3 The adsorption energies (E_{ads}),the nearest S-Cr bond length between CrB_6 and Li_2S_n (d_{S-Cr}), the shortest Li-S bond length in Li_2S_n (d_{Li-S}), and charge transfers between S_8, LiPS species (ΔQ) and CrB_6 monolayer.

Li_2S_n	E_{ads} (eV)	d_{Li-S} (Å)	d_{S-Cr} (Å)	ΔQ (e)
Li_2S_8	9.06	2.586	2.146	-0.483
Li_2S_6	5.27	2.605	2.259	-0.097
Li_2S_4	5.56	2.514	2.108	-0.351
Li_2S_2	6.36	2.621	2.087	-0.326
Li_2S	5.64	2.659	2.131	-0.071
S_8	4.03	N/A	2.273	0.116

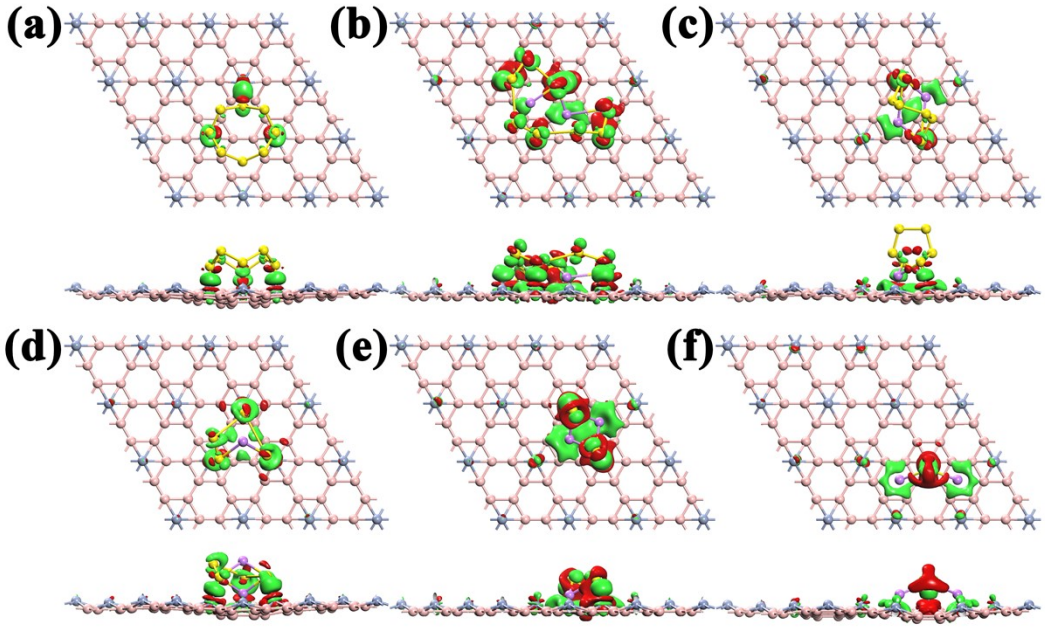

Figure S10. Top and side views of the charge density difference between (a) S_8, (b) Li_2S_8, (c) Li_2S_6, (d) Li_2S_4, (e) Li_2S_2, (f) Li_2S and CrB_6. Green and red represent charge depletion and gain, respectively.